Editors' Suggestion | Featured in Physics

Changing Flows Balance Nutrient Absorption and Bacterial Growth along the Gut

Agnese Codutti,[1] Jonas Cremer,[2] and Karen Alim[3,1,*]
[1]*Max Planck Institute for Dynamics and Self-Organization, 37077 Göttingen, Germany*
[2]*Biology Department, Stanford University, Stanford, 94305 California, USA*
[3]*Physics Department and CPA, Technische Universität München, 85748 Garching, Germany*

(Received 16 February 2022; accepted 24 August 2022; published 23 September 2022)

Small intestine motility and its ensuing flow of luminal content impact both nutrient absorption and bacterial growth. To explore this interdependence we introduce a biophysical description of intestinal flow and absorption. Rooted in observations of mice we identify the average flow velocity as the key control of absorption efficiency and bacterial growth, independent of the exact contraction pattern. We uncover self-regulation of contraction and flow in response to nutrients and bacterial levels to promote efficient absorption while restraining detrimental bacterial overgrowth.

DOI: 10.1103/PhysRevLett.129.138101

The gut microbiota strongly influences intestinal functioning and general health [1–3]. While most bacteria are located in the large intestine [4–9], bacteria are also present in the small intestine (SI) where they exert a strong effect on the host. Too high bacterial densities in the SI are particularly problematic as they cause among other symptoms pain, cephalea, chronic fatigue, bloating, and malnutrition [10]. To avoid this small intestine bacterial overgrowth syndrome luminal flow, i.e., flow of gut content, and active transport via gut muscle contractions is essential [10]. Gut motility, i.e., contractions of gut muscles [11–14], further affects nutrient absorption, while motility patterns vary, with peristalsis prevalent during starvation [11–19] and the "checkerboardlike" segmentation pattern during digestion [11–14]. From a physics perspective, gut motility drives fluid flows [15,16], thus impacting dispersion and transport of solutes [20–23]. Gut motility may therefore control nutrient absorption and bacterial densities [17] with all processes being highly intertwined. Bacteria, for example, influence nutrient levels as they compete with the gut for their absorption, and both nutrient availability and bacterial densities feed back onto gut motility [11,13,14,24,25] [Fig. 1(a)]. While motility driven flow [26–40], peristalsis-induced nutrient absorption [41–43], and bacterial growth [17] have been independently investigated, the complex dynamics arising due to different motility patterns and feedback from bacteria or nutrient density remains unknown.

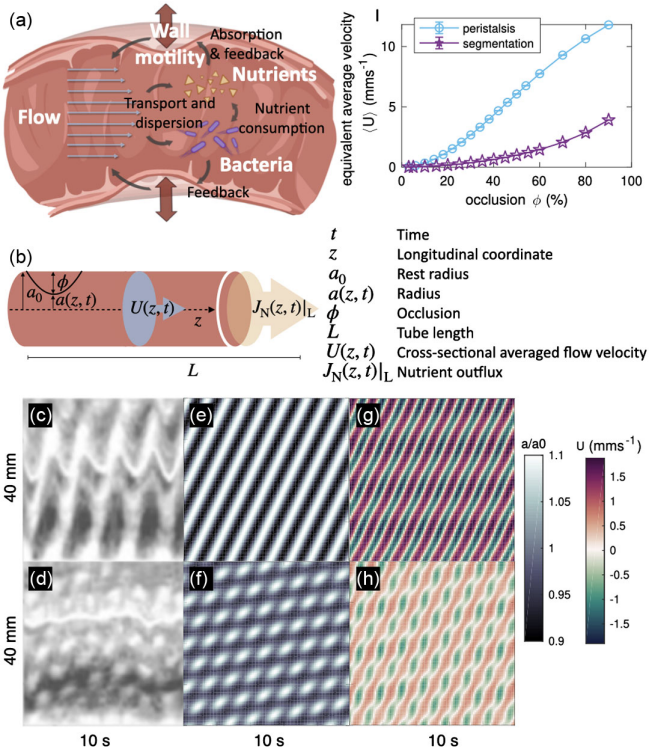

FIG. 1. Gut motility determines flows. (a) The gut is a muscular tube, whose motility patterns induce flows that affect the abundance of nutrients and bacteria. Abundances, in turn, feed back on motility. (b) Mathematical notation. (c) and (d) *In vitro* spatio-temporal map of the contraction amplitude observed for the small intestine of mice, during peristalsis and segmentation [14], respectively. Data from Ref. [14], "Motor patterns of the small intestine explained by phase-amplitude coupling of two pacemaker activities: the critical importance of propagation velocity," [14], used with permission. (e) and (f) Simulated contraction amplitudes $a(t,z)/a_0$ with 10% occlusion and (g) and (h) the emerging flow U for peristalsis and segmentation. (i) Equivalent average flow velocity $\langle U \rangle$ as function of occlusion ϕ for peristalsis (blue) and segmentation (purple). (a) Courtesy of Sara Gabrielli.

Here, we investigate the interdependence of flow, nutrient absorption, and bacterial growth for a diverse set of motility patterns. To gain analytical insights, we extend the Taylor dispersion approach [20–23,44,45] and set up a model that accounts for spatiotemporally contracting walls, the distribution of nutrients dispersed by the flow and absorbed at the gut wall, and bacterial growth. We explore the experimentally well-studied mouse gut as a reference scenario and identify the average flow velocity as the key driver of absorption and bacterial growth dynamics independent of the underlying motility pattern causing flow. We show that physiological feedback precisely controls flow velocity to balance nutrient absorption and bacterial growth.

To account for the variety of contractility patterns changing over time t and along the intestine's longitudinal direction z, we describe the variation of the gut radius $a(z,t)$ around a rest radius a_0 [Fig. 1(b)] as a superposition of two sine waves with high H and low L frequencies [14]

$$a(z,t) = a_0\{1 + \phi[\Gamma_L \sin(\xi_L) + \Gamma_H \sin(\xi_H) + \Gamma_P \sin(\xi_H)\cos(\xi_L - \theta)]\}. \quad (1)$$

Here, ϕ denotes the occlusion, i.e., the maximal percentage of radius change, $\xi := \Omega t - Kz$, Ω and K are temporal and spatial frequencies, with $\Omega_H > \Omega_L$ and $K_H > K_L$, θ is the phase shift between the high and low frequency wave, and Γ are coefficients normalized such that the factor multiplied with ϕ, i.e., the overall occlusion depth, is at maximum one. Therefore, a is bounded to $a_0 \pm a_0\phi$. Two prominent contractility patterns observed in mice [12] are represented by this function, i.e., peristalsis for $\Gamma_P = \Gamma_L = 0$, $\Gamma_H = 1$ [Figs. 1(c) and 1(e)], and segmentation for all coefficients nonzero $\Gamma_P = 0.48, \Gamma_L = 1$, $\Gamma_H = 0.78$ [14] [Figs. 1(d), 1(f), and 1(i) and Sec. 1 of Supplemental Material [46]]. For the long slender geometry of the small intestine, the flow of cross-sectionally averaged velocity U [Fig. 1(b)] is described by Stokes flow following directly from the tube's spatiotemporal contractions, the applied pressure drop Δp along the tube of length L, and the fluid's viscosity μ [16] (Sec. II, Supplemental Material [46]). To describe nutrient N and bacterial concentration B, we assume that flow in the gut is quasilaminar, i.e., $a_0 \ll K/(2\pi)$, that concentration gradients across the tube's cross section average out quickly by diffusion with diffusivity k, i.e., $(Ua^2/kL) < 1$ (Taylor limit), and that nutrient absorption is small, i.e., $\gamma a/k < 1$ with γ being the absorption strength. These conditions are approximately met for experimental parameters derived from the mouse model [14,17,47–50], under the assumption of small occlusion and water viscosity (Secs. I and III [46]). Radial mixing due to wall contractions [51] expedites radial averaging, hinting to the extension of our description beyond $(Ua^2/kL) < 1$. We derive the spatiotemporal dynamics for the cross-sectionally averaged concentrations of nutrients and bacteria within the framework of Taylor dispersion employing the invariant manifold method [20–23,44,45] for an absorbing tube wall undergoing spatiotemporal contractions (derivation in Sec. IV, numerical details in Sec. V of [46]). We expand to second order in $\epsilon = (Ua^2/kL) < 1$ with $\gamma a/k < 1$. Using Monod kinetics to describe bacterial growth [17,52,53], the dynamics of the nutrient concentration N is

$$\frac{\partial N}{\partial t} = -\gamma_{\text{eff}} N - U_{\text{eff}} \frac{\partial N}{\partial z} + k_{\text{eff}} \frac{\partial^2 N}{\partial z^2} - \alpha_{\text{BN}} B \frac{N}{N + \bar{N}}, \quad (2)$$

where $\bar{N}$ denotes the nutrient concentration below which growth is hindered [17,52,53], and α_{BN} is the bacterial nutrient consumption rate. The effective components are

$$\gamma_{\text{eff}}(t,z) = 2\frac{\gamma}{a}\left(1 - \frac{\gamma a}{4k} - \frac{1}{24k}\frac{\partial a^2}{\partial t} + \frac{U}{48k}\frac{\partial a^2}{\partial z}\right), \quad (3)$$

$$U_{\text{eff}}(t,z) = U\left(1 + \frac{\gamma a}{6k} - \frac{k}{Ua^2}\frac{\partial a^2}{\partial z} + \frac{1}{24k}\frac{\partial a^2}{\partial t}\right), \quad (4)$$

$$k_{\text{eff}}(t,z) = k\left(1 + \frac{a^2U^2}{48k^2}\right). \quad (5)$$

The corresponding equation for bacteria B is

$$\frac{\partial B}{\partial t} = -U_{\text{eff}}\Big|_{\gamma=0}\frac{\partial B}{\partial z} + k_{\text{eff}}\frac{\partial^2 B}{\partial z^2} + \alpha_g \frac{N}{N + \bar{N}} B, \quad (6)$$

where α_g is the bacterial growth rate. Equations (2)–(6) are employed in all simulations.

To assess the effect of gut contractility on ensuing flow, we consider the two prominent contractility patterns, peristalsis [Figs. 1(c) and 1(e)] and segmentation [Figs. 1(d) and 1(f)]. At equal tube occlusion, peristalsis produces stronger and more persistent longitudinal flows [Fig. 1(g)] than segmentation [Fig. 1(h)]. The equivalent average flow velocity over a period of contraction $\langle U\rangle := \langle a^2U\rangle/a_0^2$ (i.e., the flow velocity that an equivalent straight tube with the same volumetric flow would have, see Sec. II in [46]) increases with tube occlusion [15,54] and is also stronger for peristalsis than segmentation [Fig. 1(i)]. Typical flow in the embryonic mouse gut is 0.1 mms^{-1} [54], consistent with segmentation. Notably, slowing down peristalsis to achieve a lower $\langle U\rangle$ is not equivalent to employing segmentation, since in the latter case longitudinal flows U are strong and occlusion ϕ is high, which is implicated in enhancing mixing [34,35,40,51,55–57]. In conclusion, the gut has different controls of flow velocity by either adapting the muscle strength that is coordinating tube occlusion or by retaining the same occlusion but modifying the spatiotemporal pattern of contractions.

To determine how different flow patterns impact nutrient dispersion and absorption, we follow the spread of a finite amount of nutrients normally distributed at time zero around $z_{\text{peak}} = L/2$, with free outflow and inflow,

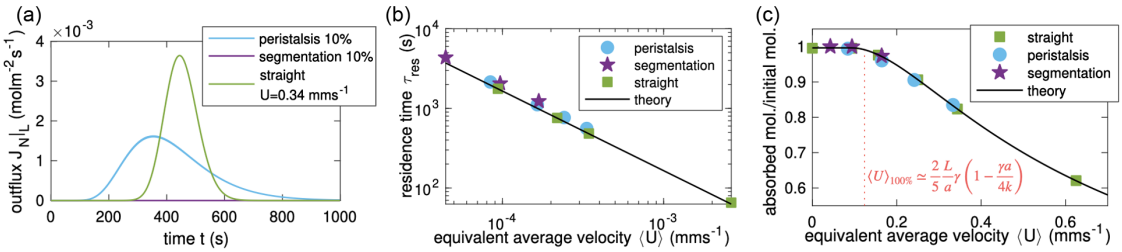

FIG. 2. Flow velocity governs residence times and nutrient absorption. Initially, nutrients are normally distributed around $z_{\mathrm{peak}} = L/2$. (a) Average outflux of nutrients for peristalsis 10% occlusion (light blue), segmentation 10% occlusion (purple), and a straight tube with the 10%-peristalsis-equivalent average flow velocity $\langle U \rangle$ (green). (b) Residence times τ_{res} as function of equivalent average flow velocity $\langle U \rangle$ for peristalsis (light blue), segmentation (purple), straight tube (green), and theory $L/(2\langle U \rangle)$ (line). (c) Total absorbed molecules during emptying time normalized by the initial molecules in the tube as function of the equivalent average flow velocity $\langle U \rangle$ for peristalsis (light blue), segmentation (purple), a straight tube (green), and theoretical prediction for a straight tube (black). The vertical line is the theoretical velocity $\langle U \rangle_{100\%}$ above which there is no complete absorption.

$\partial N/\partial z|_{\mathrm{boundary}} = 0$, in the absence of bacteria. In agreement with experimental observations [58], nutrient dispersion is directly modulated by the contraction patterns as illustrated by the outflow behavior shown in Fig. 2(a). Yet, we observe that the residence time $\tau_{\mathrm{res}} := \int dt(tJ_N|_L)/\int dtJ_N|_L$, with $J_N|_L \sim [a^2UN - a^2k_{\mathrm{eff}}(\partial N/\partial z)]_{z=L}$ the approximated flux at the outlet [23] [Sec. VI of [46] and Fig. 1(b)], is independent of the local variations in the flow field incorporated by the different patterns, but only depends on the equivalent average flow velocity $\tau_{\mathrm{res}} = z_{\mathrm{distance}}/\langle U \rangle$, where $z_{\mathrm{distance}} = L - z_{\mathrm{peak}} = L/2$ is the distance the nutrients travel before exiting [Fig. 2(b)]. The same pattern independence applies for the nutrient absorption rate $\Phi_N := -\int_S (k\nabla N)_\perp dS$ (mol s^{-1}) across the tube's surface S (Sec. VII [46]). In fact, we derive analytically that its decay rate is τ_{abs}, which is by definition the characteristic absorption timescale, shown to be to good approximation $\tau_{\mathrm{abs}} = \gamma_{\mathrm{eff}}^{-1}|_{a=a_0}$ for all motility patterns (Secs. VIII and IX [46]). Therefore, the efficiency, defined as the total amount of absorbed molecules until the tube empties, normalized by the initial amount of molecules $\int_{5\tau_{\mathrm{res}}} \Phi_N dt/N_{\mathrm{initial}}$, is pattern independent [Fig. 2(c)]. The emptying time is defined as $5\tau_{\mathrm{res}}$, since it corresponds to a leftover of $N/N_0 = 0.0067\%$.

Given this result, we deduce that, for small velocities $\langle U \rangle_{100\%} \leq (L/5\tau_{\mathrm{abs}}) = \frac{2}{5}(L/a)\gamma[1 - (\gamma a/4k)]$ that allow for the residence time to be longer than the absorption time $\tau_{\mathrm{res}} > \tau_{\mathrm{abs}}$, 100% nutrient absorption efficiency can be reached, independent of the flow-generating contractility pattern [red vertical line in Fig. 2(c)]. When considering only the gut's role to absorb nutrients, low flow velocities below $\langle U \rangle_{100\%}$ seem ideal [11,27]. Yet, we have so far neglected the impact of flow on bacterial concentration.

Modeling the stomach as an upheld reservoir of a fixed concentration of bacteria and nutrients $N|_0 = N_0$, $B|_0 = B_0$ and allowing free outflow $\partial N/\partial z|_L = 0$ [17], we analytically solve for both nutrient and bacteria dynamics at steady state $\langle \partial N/\partial t \rangle = 0$, $\langle \partial B/\partial t \rangle = 0$ for a straight tube (see Sec. X [46]). Employing that wall absorption dominates over bacterial consumption terms in Eq. (2) $\gamma_{\mathrm{eff}} N \gg \alpha_{\mathrm{BN}} BN/(N + \bar{N})$ and neglecting the diffusion term, which yields an error $< 0.6\%$ (Sec. X D [46]), we obtain for the nutrients N and bacteria B currently in the gut

$$\frac{N}{N_0} = \exp\left(-\frac{\tau_{\mathrm{res}}}{\tau_{\mathrm{abs}}}\frac{z}{L}\right), \tag{7}$$

$$\frac{B}{B_0} = \left(\frac{1 + \frac{\bar{N}}{N_0}}{\frac{\bar{N}}{N_0} + \exp\left(-\frac{\tau_{\mathrm{res}}}{\tau_{\mathrm{abs}}}\frac{z}{L}\right)}\right)^{\tau_{\mathrm{abs}}/\tau_g}, \tag{8}$$

where we approximated $U_{\mathrm{eff}} \sim U = L/\tau_{\mathrm{res}}$ given the small absorption strength $\gamma a/k < 1$, and where we defined the growth time as $\tau_g := \alpha_g^{-1}$. Here $\tau_{\mathrm{res}} = L/\langle U \rangle$, since the nutrients enter at the inlet and travel $z_{\mathrm{distance}} = L$ before exiting. This analytical result, in qualitative agreement with previous simulations [17], clearly states that nutrient concentration is regulated by the competition between advection and absorption timescales. Bacterial concentration is additionally controlled by the competition between nutrient absorption τ_{abs} and bacterial growth set by the timescale τ_g, with high bacterial numbers arising for large $\tau_{\mathrm{abs}}/\tau_g$, i.e., when bacteria multiply much faster than the depletion of nutrients via absorption.

Which of these timescales τ_g, τ_{abs}, and τ_{res} does the gut regulate to improve absorption and limit bacterial growth? For a finite nutrient amount we found that the residence time, which is governed by the equivalent average flow, is the most important timescale determining absorption [Fig. 2(c)]. Indeed, this is also true here, independent of the motility pattern, for the steady state with an upheld concentration of both nutrients and bacteria as confirmed by simulations. The equivalent flow velocity is regulating the absorption rate Φ_N [Fig. 3(a): rate normalized by the straight tube infinite-velocity limit $\Phi_{U\,\mathrm{inf}} = 2\pi kLC_0\gamma(1 - \gamma/4)(1 + \gamma/6)(1 + \gamma/12)^{-1}$, which is independent of flow velocity and nutrient influx and thus of the motility pattern; see Sec. X of [46]]. In apparent contrast to the case of a finite amount of

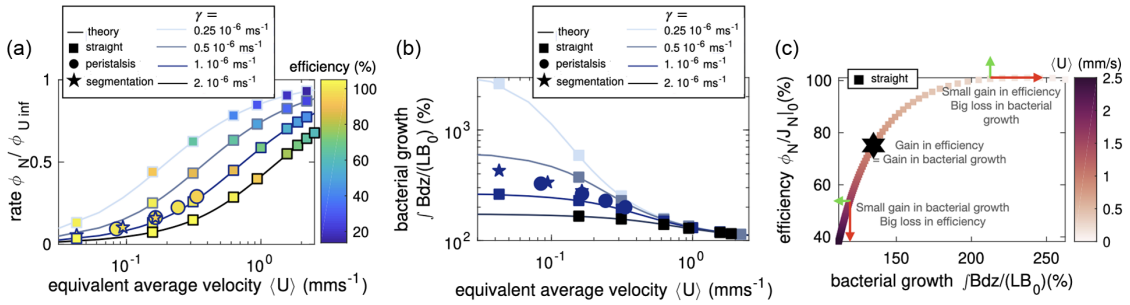

FIG. 3. Nutrients' absorption and bacterial growth need to be balanced. Comparison between straight tube theory (lines) and simulations (squares for straight tube, circle for peristalsis, and pentagram for segmentation) of the (a) normalized absorption rate $\Phi_N/\Phi_{U\,\mathrm{inf}}$ and (b) bacterial growth $\int_0^L Bdz/(LB_0)$ as function of the equivalent average flow velocity $\langle U\rangle$, at steady state with upheld concentration at the inlet. Different absorption strength γ are given (from dark to light blue, respectively 2×10^{-6}, physiological parameter 1×10^{-6}, 0.5×10^{-6}, 0.25×10^{-6} ms^{-1}). In (a), data points are color coded by the steady-state efficiency $\Phi_N/(J_N|_0)$. (c) Theoretical steady-state efficiency vs bacterial growth for a straight tube with upheld concentration, color coded by the equivalent average flow velocity $\langle U\rangle$. The hexagram is the optimal point ($\langle U\rangle = 0.88$ mm s^{-1}), simultaneously optimizing the efficiency (74%) and the bacterial growth (134%).

nutrients, higher flows correspond to better absorption. However, this is due to the higher inflow of nutrients into the gut when flow increases. This explains why in Eq. (7) the nutrients in the tube N/N_0 decrease for longer τ_{res}: slower flows mean longer residence time but fewer nutrients entering. Indeed, the efficiency given as the absorption rate normalized by the influx $(\Phi_N/J_N|_0)$ confirms our previous result that higher flows have a much lower efficiency, reaching 100% only for low velocities, in agreement with Ref. [27]. Flow is also regulating bacterial abundance $\int_0^L Bdz/(LB_0)$ [Fig. 3(b) and Sec. X of [46]], hindering it at high velocities and favoring it at small velocities. We confirm that nutrient absorption and bacterial growth are largely pattern independent [Figs. 3(a) and 3(b)], with good agreement between simulations and the straight tube theory, and that the system's dynamics is again dominated by the equivalent average flow as key parameter. Another regulatory parameter is the absorption strength γ, with higher γ promoting higher absorption efficiency [Fig. 3(a)] and less bacterial growth [Fig. 3(b)]. Because of the normalization $\Phi_{U\,\mathrm{inf}}$ a higher absorption strength γ corresponds to a smaller nondimensional absorption rate $\Phi_N/\Phi_{U\,\mathrm{inf}}$ and a higher-dimensional absorption rate Φ_N (Sec. X B [46]). Notably, the physiological absorption strength $\gamma = 10^{-6}$ ms^{-1} [17] retains an efficiency of at least 40% even for the unfavorable case of fast flows, while it strongly limits bacterial growth, never surpassing 270% even at slow flows.

The small intestine of mice appears to operate in a parameter range where changing the motility pattern, and thus the flow velocity, is an efficient mechanism to promote nutrient absorption and limit bacterial growth. Yet, does an optimal flow velocity exist? Plotting the theoretical steady-state efficiency as a function of bacterial growth for a straight tube with upheld concentration [Fig. 3(c)], we define the optimum as the point where the curve derivative $\delta\mathrm{efficiency}/\delta B$ is equal to 1 (at $\langle U\rangle = 0.88$ mm s^{-1}). Moving from that point by increasing flow slightly favors bacterial reduction but significantly worsens nutrient absorption, with the opposite when flow decreases. While this optimal velocity does not fully optimize both aims, it might provide an acceptable value for both of them simultaneously (74% efficiency, 134% bacterial growth). These results suggest that a better strategy might be to alternate between two flow phases, with slow flow during segmentation to fully optimize absorption and fast flows during peristalsis to down-regulate bacteria. Experimental observations [11,12,27,59] support such alternations in coordination with meal intake and fasting.

It remains an open question whether the switch between segmentation (duration $T_{\mathrm{abs\ phase}}$) and peristalsis ($T_{\mathrm{clean\ phase}}$) is rather driven by nutrient availability [11,13,14,24] or bacterial abundance [25] (Sec. XI [46]). To answer, we compare the system's timescales (Sec. XI B [46]). From the perspective of maximizing absorption after a meal, flow needs to be slow enough ($\tau_{\mathrm{abs}} \ll \tau_{\mathrm{res}}^{\mathrm{seg}}$) for a long enough duration ($\tau_{\mathrm{abs}} \ll T_{\mathrm{abs\ phase}}$) to maintain nutrients in the gut and allow for absorption. Since meals are of finite size, the gut's aim is to achieve high efficiency to minimize nutrient loss. To regulate bacterial numbers, flow needs to be fast enough such that the residence time is shorter than the bacterial growth timescale ($\tau_{\mathrm{res}}^{\mathrm{per}} \ll \tau_g$) and last long enough to flush out the desired amount of bacteria ($T_{\mathrm{clean\ phase}} \simeq \tau_{\mathrm{res}}^{\mathrm{per}}$). While pathogenic bacteria are ideally completely washed out, also commensal bacteria should be down-regulated to avoid overgrowth. In principle, a very long absorption phase can clean out bacteria, since eventually nutrients are so scarce that bacterial growth is inhibited and bacteria are slowly flushed out (Fig. 4). This is, however, a very risky strategy as an early arrival of a new meal before the completion of a slow washout may

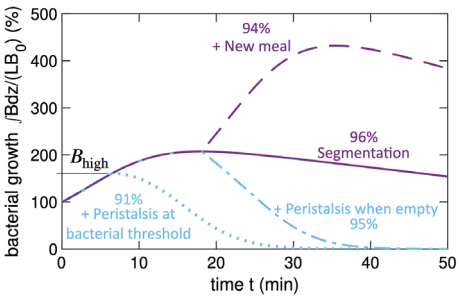

FIG. 4. Alternating patterns improve efficiency and bacterial regulation. Absorption phase (segmentation 10%, initially uniformly nutrient and bacteria-filled tube, no inflow, free outflow, purple filled line, and Sec. XI of [46]) reaches 96% of efficiency. Adding a meal (at 18 min) triggers strong bacterial growth (purple dashed line). Switching to fast flows (peristalsis 10%) when the tube is empty (94% of absorbed molecules, peak of bacterial population) quickly decreases the bacterial number (blue mixed line). Starting peristalsis above a threshold of bacterial growth $B_{\text{high}} = 160\%$ implies higher loss of efficiency at 91% (blue dotted line).

result in bacterial overgrowth, with bigger meals worsening bacterial growth (Sec. XI D [46]). Instead of being indefinite, the absorption phase is thus only maintained temporarily and the flow-pattern switch is coordinated depending on the state of the system. In particular, if bacterial growth is very slow compared to the absorption and residence timescales ($\tau_{\text{abs}} \ll \tau_{\text{res}}^{\text{seg}} \ll \tau_g$ or $\tau_{\text{abs}} \ll \tau_g \leq \tau_{\text{res}}^{\text{seg}}$), the absorption phase maximizes the efficiency while keeping at bay bacterial growth if it lasts $T_{\text{abs phase}} \simeq \tau_{\text{res}}^{\text{seg}}$. A feedback control in which the nutrients' depletion triggers peristaltic cleaning appears to be sufficient to quickly reduce bacteria while ensuring high efficiency (Fig. 4). In fact, nutrients trigger slow flows thanks to pressure or receptors' sensing [11,13,24], thus their absence might lead to fast phases [11]. If, instead, bacterial growth is very quick ($\tau_g \ll \tau_{\text{abs}} \ll \tau_{\text{res}}^{\text{seg}}$), overgrowth is eminent if $T_{\text{abs phase}} \simeq \tau_{\text{res}}^{\text{seg}}$. Here, a feedback control in which high bacterial densities trigger peristalsis and limit absorption phase below a duration $T_{\text{abs phase}} \leq \tau_g \ll \tau_{\text{abs}} \ll \tau_{\text{res}}^{\text{seg}}$ is required to limit bacteria growth. This control is provided by bacterial metabolites, which trigger enhanced motility through gut receptors [25]. This comes at the cost of reduced efficiency, which can be counteracted by maximizing $(\tau_g + \tau_{\text{res}}^{\text{per}})/\tau_{\text{abs}}$ (Secs. XI A–C [46]). Increasing the bacterial threshold that triggers fast flows allows for longer absorption phases and higher efficiency (Sec. XI D [46]). For the healthy mouse gut, $\tau_{\text{abs}} < \tau_g$ holds (Sec. III [46]) and a feedback control via nutrients appears to be efficient. However, disease and other disruptions may affect this parameter balance and require a feedback control via bacteria—at least as a backup option. In conclusion, our mapping to experimental measures of simple timescales provides a direct interface to experiments and promotes an integrative understanding of the intestinal physiological processes.

The source code, analysis code and the data are available at [60].

We thank Sophie Marbach for discussions on Taylor dispersion. The work was supported by the Max-Planck-Gesellschaft.

*k.alim@tum.de

[1] S. El Aidy, B. van den Bogert, and M. Kleerebezem, Curr. Opin. Biotechnol. **32**, 14 (2015).
[2] J. F. Cryan, K. J. O'Riordan, C. S. M. Cowan, K. V. Sandhu, T. F. S. Bastiaanssen, M. Boehme, M. G. Codagnone, S. Cussotto, C. Fulling, A. V. Golubeva *et al.*, Physiol. Rev. **99**, 1877 (2019).
[3] C. Willyard, Nature (London) **590**, 22 (2021).
[4] A. S. Moorthy, S. P. J. Brooks, M. Kalmokoff, and H. J. Eberl, PLoS One **10**, e0145309 (2015).
[5] H. Kettle, P. G. H. Louis, G. Holtrop, S. H. Duncan, and H. J. Flint, Environ. Microbiol. **17**, 1615 (2015).
[6] H. Kettle, G. Holtrop, P. G. H. Louis, and H. J. Flint, Methods Ecol. Evol. **9**, 399 (2018).
[7] S. Labarthe, B. Polizzi, T. Phan, T. Goudon, M. Ribot, and B. Laroche, J. Theor. Biol. **462**, 552 (2019).
[8] S. Le Feunteun, A. Al-Razaz, M. Dekker, E. George, B. Laroche, and G. van Aken, Annu. Rev. Food Sci. Technol. **12**, 149 (2021).
[9] D. Labavić, C. Loverdo, and A. F. Bitbol, Proc. Natl. Acad. Sci. U.S.A. **119**, e2108671119 (2022).
[10] A. C. Dukowicz, B. E. Lacy, and G. M. Levine, Gastroenterol. Hepatol. (N.Y.) **3**, 112 (2007).
[11] K. E. Barrett, S. M. Barman, J. Yuan, and H. L. Brooks, *Ganong's Review of Medical Physiology*, 25th ed. (McGraw-Hill Education, New York, 2016).
[12] J. D. Huizinga and W. J. E. P. Lammers, Am. J. Physiol. Gastrointest. Liver Physiol. **296**, G1 (2009).
[13] J. D. Huizinga, J. H. Chen, Y. F. Zhu, A. Pawelka, R. J. McGinn, B. L. Bardakjian, S. P. Parsons, W. A. Kunze, R. Y. Wu, P. Bercik *et al.*, Nat. Commun. **5**, 3326 (2014).
[14] J. D. Huizinga, S. P. Parsons, J. H. Chen, A. Pawelka, M. Pistilli, C. Li, Y. Yu, P. Ye, Q. Liu, M. Tong *et al.*, Am. J. Physiol. Cell Physiol. **309**, C403 (2015).
[15] A. H. Shapiro, M. Y. Jaffrin, and S. L. Weinberg, J. Fluid Mech. **37**, 799 (1969).
[16] M. Li and J. G. Brasseur, J. Fluid Mech. **248**, 129 (1993).
[17] T. Ishikawa, T. Sato, G. Mohit, Y. Imai, and T. Yamaguchi, J. Theor. Biol. **279**, 63 (2011).
[18] J. Jiménez-Lozano, M. Sen, and P. F. Dunn, Phys. Rev. E **79**, 041901 (2009).
[19] J. Jiménez-Lozano and M. Sen, Phys. Fluids **22**, 043303 (2010).
[20] G. I. Taylor, Proc. R. Soc. A **219**, 186 (1953).
[21] G. I. Taylor, Proc. R. Soc. A **223**, 446 (1954).
[22] R. Aris, Proc. R. Soc. A **235**, 67 (1956).
[23] S. Marbach and K. Alim, Phys. Rev. Fluids **4**, 114202 (2019).
[24] T. E. Moxon, P. Nimmegeers, D. Telen, P. J. Fryer, J. Van Impe, and S. Bakalisa, Chem. Eng. Sci. **171**, 318 (2017).

[25] B. Waclawiková, A. Codutti, K. Alim, and S. El Aidy, Gut Microbes **14**, 1997296 (2022).
[26] B. Jeffrey, H. S. Udaykumar, and K. S. Schulze, Am. J. Physiol. Gastrointest. Liver. Physiol. **285**, G907 (2003).
[27] J. G. Brasseur, G. G. Banco, A. C. Ailiani, Y. Wang, T. Neuberger, N. B. Smith, and A. G. Webb, Motility and absorption in the small intestines: Integrating MRI with lattice Boltzmann models, in *2009 IEEE International Symposium on Biomedical Imaging: From Nano to Macro* (IEEE, Boston, MA, 2009), p. 374.
[28] Y. Wang, J. G. Brasseur, G. G. Banco, A. G. Webb, A. C. Ailiani, and T. Neuberger, Phil. Trans. R. Soc. A **368**, 2863 (2010).
[29] M. R. Jaime Fonseca, Ph.D. thesis, University of Birmingham, 2011.
[30] D. Tripathi, Math. Biosci. **233**, 90 (2011).
[31] R. G. Lentle, C. De Loubens, C. Hulls, P. W. M. Janssen, M. D. Golding, and J. P. Chambers, Neurogastroenterol. Motil. **24**, 686 (2012).
[32] C. de Loubens, R. G. Lentle, R. J. Love, C. Hulls, and P. W. M. Janssen, J. R. Soc. Interface **10**, 20130027 (2013).
[33] R. J. Love, R. G. Lentle, P. Asvarujanon, Y. Hemar, and K. J. Stafford, Food Digestion **4**, 26 (2013).
[34] L. Fullard, W. Lammers, G. C. Wake, and M. J. Ferrua, Food Funct. **5**, 2731 (2014).
[35] L. A. Fullard, W. J. Lammers, and M. J. Ferrua, J. Food Eng. **160**, 1 (2015).
[36] M. D. Sinnott, P. W. Cleary, and S. M. Harrison, Appl. Math. Model. **44**, 143 (2017).
[37] S. Muttakin, T. E. Moxon, and O. Gouseti, *In vivo, In vitro, and In silico Studies of the GI Tract in Interdisciplinary Approaches to Food Digestion*, edited by O. Gouseti, G. M. Bornhorst, S. Bakalis, and A. Mackie (Springer International Publishing, New York, 2019), pp. 29–67.
[38] R. K. Avvari, *Biomechanics of the Small Intestinal Contractions in Digestive System—Recent Advances*, edited by X. Qi and S. Koruth (IntechOpen, London, 2019).
[39] S. Le Feunteun, A. R. Mackie, and D. Dupont, Curr. Opin. Food Sci. **31**, 121 (2020).
[40] J. Zha, S. Zou, J. Hao, X. Liu, G. Delaplace, R. Jeantet, D. Dupont, P. Wu, X. D. Chen, and J. Xiao, Chem. Eng. Sci. **229**, 116079 (2021).
[41] M. Taghipoor, P. Lescoat, J. R. Licois, C. Georgelin, and G. Barles, J. Theor. Biol. **294**, 114 (2012).
[42] M. Taghipoor, G. Barles, C. Georgelin, J. R. Licois, and P. Lescoat, Math. Biosci. **258**, 101 (2014).
[43] J. S. Karthikeyan, D. Salvi, and M. V. Karwe, J. Food Eng. **292**, 110339 (2021).
[44] G. N. Mercer and A. J. Roberts, SIAM J. Appl. Math. **50**, 1547 (1990).
[45] G. N. Mercer and A. J. Roberts, Jpn. J. Ind. Appl. Math. **11**, 499 (1994).
[46] See Supplemental Material at http://link.aps.org/supplemental/10.1103/PhysRevLett.129.138101. Section I for the derivation of the generalized motility pattern. Section II for flow calculations. Section III for parameter choice. Section IV for derivation of the Taylor dispersion equations. Section V for numerical details. Section VI for flux derivation and boundary conditions. Section VII for the definition of the absorption rate. Section VIII for the theoretical solution of the a nutrient Gaussian experiment. Section IX for the absorption time. Section X for steady-state solution. Section XI for feedback mechanisms.
[47] A. Pereira de Souza, R. Sieberg, H. Li, H. R. Cahill, D. Zhao, T. C. Araújo-Jorge, H. B. Tanowitz, and L. A. Jelicks, Parasitology research **106**, 1293 (2010).
[48] H. Ohkubo, T. Kessoku, A. Fuyuki, H. Iida, M. Inamori, T. Fujii, H. Kawamura, Y. Hata, N. Manabe, T. Chiba *et al.*, Am. J. Gastroenterol. **108**, 1130 (2013).
[49] T. E. Moxon, O. Mihailova, O. Gouseti, P. J. Frye, and S. Bakalis, Engineering digestion: Effect of viscosity and gastric secretions on the absorption of nutrients, in *Gums and Stabilisers for the Food Industry 18: Hydrocolloid Functionality for Affordable and Sustainable Global Food Solutions* (The Royal Society of Chemistry, London, 2016), p. 264.
[50] F. Hugenholtz and W. M. de Vos, Cell Mol. Life Sci. **75**, 149 (2018).
[51] R. G. Lentle and P. W. M. Janssen, J. Comp. Physiol. B **178**, 673 (2008).
[52] J. Gerritse, F. Schut, and J. C. Gottschal, Appl. Environ. Microbiol. **58**, 1466 (1992).
[53] K. A. Johnson and R. S. Goody, Biochemistry **50**, 8264 (2011).
[54] R. J. Amedzrovi Agbesi and N. R. Chevalier, Phys. Rev. Fluids **7**, 043101 (2022).
[55] R. G. Lentle, P. W. M. Janssen, C. Deloubens, Y. F. Lim, C. Hulls, and P. Chambers, Neurogastroenterology and motility : the official Journal of the European Gastrointestinal Motility Society **25**, 881 (2013).
[56] R. G. Lentle and C. de Loubens, J. Comp. Physiol. B **185**, 369 (2015).
[57] M. Schütt, K. Stamatopoulos, M. J. H. Simmons, H. K. Batchelor, and A. Alexiadis, Comput. Biol. Med. **121**, 103819 (2020).
[58] P. W. M. Janssen, R. G. Lentle, P. Asvarujanon, P. Chambers, K. J. Stafford, and Y. Hemar, J. Physiol. **582**, 1239 (2007).
[59] E. Deloose, P. Janssen, I. Depoortere, and J. Tack, Nat. Rev. Gastroenterol. Hepatol. **9**, 271 (2012).
[60] Data, source code and analysis code available at 10.14459/2022MP1686728.